Torsion-vibration interactions in hydrogen peroxide. 1. Calculation of the trans barrier for OH overtone excitations up to v = 8

ARTICLE *in* THE JOURNAL OF PHYSICAL CHEMISTRY · JULY 1988

Impact Factor: 2.78 · DOI: 10.1021/j100326a012

2 AUTHORS:

John E Carpenter
University of Iowa
40 PUBLICATIONS **1,919** CITATIONS
SEE PROFILE

Frank Weinhold
University of Wisconsin–Madison
199 PUBLICATIONS **29,050** CITATIONS
SEE PROFILE

Torsion–Vibration Interactions in Hydrogen Peroxide. 1. Calculation of the Trans Barrier for OH Overtone Excitations up to $v = 8$[1]

J. E. Carpenter and F. Weinhold*

Theoretical Chemistry Institute and Department of Chemistry, University of Wisconsin—Madison, Madison, Wisconsin 53706 (Received: November 2, 1987)

We have employed high-level ab initio calculations to investigate torsion–vibration coupling in hydrogen peroxide for high overtone excitations of OH stretch. We obtain good agreement with the experimental results of Dübal and Crim on the increase of the H_2O_2 trans barrier with increasing levels of overtone excitation. Although such an increase is surprising from a steric repulsions point of view, we find that the effect can be numerically reproduced on the basis of potential energy coupling between adiabatically separable torsion–vibration states. Using a local mode model for the OH overtone excitation, we compute the v-dependent trans barrier by averaging the computed trans barrier over local mode wave functions, reducing the required portion of the potential energy surface to two one-dimensional slices. This reduction makes it feasible to employ the highly polarized extended basis sets [up to 6-311G(3d,2p)] and high level of correlation treatment (MP2 and GVB) needed to describe the torsional properties of H_2O_2 accurately. While the absolute magnitude of the trans barrier is very sensitive to the level of calculation, we find that the change in trans barrier upon overtone excitation is adequately reproduced at much lower levels of theory.

I. Introduction

The infrared spectrum of hydrogen peroxide can be successfully analyzed by assuming that the low-frequency torsional motion (χ) is governed by an effective one-dimensional wave equation of the form

$$[\hat{T}_\chi + \hat{\mathcal{V}}_v^{(\mathrm{eff})}(\chi)]\Xi_{vm}(\chi) = E_{vm}\Xi_{vm}(\chi) \qquad \text{(I.1)}$$

with torsional wave function $\Xi_{vm}(\chi)$ and eigenvalue E_{vm} for torsional quantum state m.[2] In this equation $\hat{\mathcal{V}}_v^{(\mathrm{eff})}(\chi)$ is the *effective* torsional potential for a particular state of excitation (labeled by quantum numbers v) associated with high-frequency vibrational coordinates s.

Experimental information concerning $\hat{\mathcal{V}}_v^{(\mathrm{eff})}(\chi)$ can be obtained by observing transitions in the vibrational spectrum associated with changes of torsional state, analogous to observing vibrational progressions in an electronic spectrum. Even the earliest such studies of H_2O_2[2a,3] indicated the importance of the v dependence of the effective torsional potential (analogous to the dependence of molecular potential energy surfaces on the state of electronic excitation) arising from torsion–vibration interactions.

Empirically, it is found that $\hat{\mathcal{V}}_v^{(\mathrm{eff})}(\chi)$ is of double-well form and can be represented by a Fourier series up to third order in cos χ, with v-dependent coefficients. The empirical Fourier coefficients can in turn be expressed in terms of the cis barrier $\mathcal{V}_v^{\mathrm{cis}} = \hat{\mathcal{V}}_v^{(\mathrm{eff})}(\chi=0)$ located at $\chi = 0$, the trans barrier $\mathcal{V}_v^{\mathrm{trans}} = \hat{\mathcal{V}}_v^{(\mathrm{eff})}(\chi = \pi)$ located at $\chi = 180°$, and the equilibrium torsional angle χ_v^{eq}. [A remaining coefficient is fixed by the condition $\hat{\mathcal{V}}_v^{(\mathrm{eff})}(\chi_v^{\mathrm{eq}}) = 0$, which establishes the zero of energy.]

Recently, Dübal and Crim[4] have extended the range of such studies by observing torsional progressions for the $v = 4$, 5, and 6 OH overtone vibrations of H_2O_2, which are believed to correspond to local mode excitations. These observations, combined with earlier work on $v = 0$–3 states, yield the surprising result that the trans barrier *increases* by about 75 cm^{-1} per quantum of OH stretch. Such studies provide remarkable new information on torsion–vibration interactions in highly excited vibrational states of H_2O_2 and challenge many assumptions concerning the nature of the forces leading to torsional barriers.

In a simple Born–Oppenheimer ("clamped torsion") approximation,[5] the full nonadiabatic wave equation for the nuclear motion

$$\hat{H}\Psi^{(\mathrm{NA})}(\mathbf{s},\chi) = E^{(\mathrm{NA})}\Psi^{(\mathrm{NA})}(\mathbf{s},\chi) \qquad \text{(I.2)}$$

is replaced by separate equations for the vibrational (s) and torsional (χ) motion,

$$[\hat{T}_\mathbf{s} + \hat{V}(\mathbf{s},\chi)]\psi_v(\mathbf{s};\chi) = \mathcal{E}_v(\chi)\,\psi_v(\mathbf{s};\chi) \qquad \text{(I.3a)}$$

$$[\hat{T}_\chi + \mathcal{E}_v(\chi)]\Xi_{vm}^{(\mathrm{BO})}(\chi) = E_{vm}^{(\mathrm{BO})}\,\Xi_{vm}^{(\mathrm{BO})}(\chi) \qquad \text{(I.3b)}$$

Here, $\hat{V}(\mathbf{s},\chi)$ is the full six-dimensional potential energy surface of H_2O_2, associated with the total Hamiltonian

$$\hat{H} = \hat{T}_\mathbf{s} + \hat{T}_\chi + \hat{V}(\mathbf{s},\chi) \qquad \text{(I.4)}$$

$\mathcal{E}_v(\chi)$ and $\psi_v(\mathbf{s};\chi)$ are the eigenvalue and eigenfunction (parametrically dependent on torsion angle χ) for the high-frequency vibrational modes s, and $E_{vm}^{(\mathrm{BO})}$, $\Xi_{vm}^{(\mathrm{BO})}$ are the corresponding quantities for the low-frequency torsion. Equations I.3a and I.3b lead to the total Born–Oppenheimer wave function

$$\Psi^{(\mathrm{BO})}(\mathbf{s},\chi) = \psi_v(\mathbf{s};\chi)\,\Xi_{vm}^{(\mathrm{BO})} \qquad \text{(I.5)}$$

and associated eigenvalue estimate $E_{vm}^{(\mathrm{BO})}$. In this approximation, the effective potential of eq I.1 is identified with the eigenvalue $\mathcal{E}_v(\chi)$ of eq I.3a

$$\hat{\mathcal{V}}_v^{(\mathrm{BO})} = \mathcal{E}_v(\chi) \qquad \text{(I.6)}$$

and the v dependence of this quantity arises from potential energy (PE) coupling terms in $\hat{V}(\mathbf{s},\chi)$ (of electronic origin) as well as kinetic energy (KE) coupling terms in $\hat{T}_\mathbf{s}$ (arising from the χ dependence of the G matrix elements).

Hirota[2a] attempted to explain the v dependence of $\hat{\mathcal{V}}_v^{(\mathrm{eff})}(\chi)$ by approximately solving eq I.3a, but his solution assumed that the torsional motion is coupled to the other modes via $\hat{T}_\mathbf{s}$ alone (a pure KE coupling effect). The $\mathcal{E}_v(\chi)$ he found predicts that the trans barrier would decrease upon overtone excitation, in direct opposition to current experimental observations. Redington et al.,[2b] citing work of Penney and Sutherland[6] and of Heath and Linnett[7] on vibrational excitation in H_2O, suggested that the torsion–vibration interaction might be due to PE coupling, but the exact nature of this coupling was not investigated in detail.

(1) Parts of this work were reported in a previous communication: Carpenter, J. E.; Weinhold, F. *J. Phys. Chem.* **1986**, *90*, 6405–6408.
(2) (a) Hirota, E. *J. Chem. Phys.* **1958**, *28*, 839–846. (b) Redington, R. L.; Olson, W. B.; Cross, P. C. *J. Chem. Phys.* **1962**, *36*, 1311–1326. (c) Hunt, R. H.; Leacock, R. A.; Peters, C. W.; Hecht, K. T. *J. Chem. Phys.* **1965**, *42*, 1931–1946.
(3) Zumwalt, L. R.; Giguere, P. A. *J. Chem. Phys.* **1941**, *9*, 458–462.
(4) Dübal, H.-R.; Crim, F. F. *J. Chem. Phys.* **1985**, *83*, 3863–3872.
(5) Born, M.; Huang, K. *Dynamical Theory of Crystal Lattices*; Oxford University Press; London, 1954; Appendix VII.
(6) Penney, W. G.; Sutherland, G. B. B. M. *J. Chem. Phys.* **1934**, *2*, 492–498.
(7) Heath, D. J.; Linnett, J. W. *Trans. Faraday Soc.* **1947**, *44*, 556–564.

0022-3654/88/2092-4295$01.50/0

Indeed, a simple steric repulsion (or "Pauli repulsions"[8]) model of internal rotation barriers might suggest that the PE-coupling terms, if present at all, would give a trend *opposite* to that seen experimentally. In such a model, barriers would be expected to *diminish* with increased OH stretch, as the average distance between "repelling" groups is increased. Thus, the observed barrier increase with increased OH stretch is somewhat paradoxical from a PE-coupling point of view and suggests that KE-coupling effects are the dominant contribution to the observed torsion–vibration interactions.

Mills[9] pointed out that additional KE-coupling effects could arise from breakdown of the Born–Oppenheimer approximation. Such coupling arises from the action of the torsional kinetic energy operator $\hat{T}_\chi$ on the parametric χ dependence of the vibrational wave function $\psi_v(\mathbf{s};\chi)$ of (I.3a), leading to a nonvanishing coupling operator of the form

$$\hat{B}_v(\chi) = \langle \psi_v | \hat{T}_\chi | \psi_v \rangle_\mathbf{s} \tag{I.7}$$

where the notation $\langle ... \rangle_\mathbf{s}$ denotes integration over high-frequency $\mathbf{s}$ coordinates only. The first-order effect of the KE-coupling operator (I.7) is to give an "adiabatic" (A) correction to the clamped-torsion Born–Oppenheimer approximation

$$\tilde{E}^{(A)}_{vm} = E^{(BO)}_{vm} + \langle \Xi^{(BO)}_{vm} | \hat{B}_v(\chi) | \Xi^{(BO)}_{vm} \rangle_\chi = \langle \Psi^{(BO)}(\mathbf{s},\chi) | \hat{H} | \Psi^{(BO)}(\mathbf{s},\chi) \rangle \tag{I.8}$$

where $\langle ... \rangle_\chi$ denotes integration over χ only. Alternately, one may introduce the KE-coupling operator (I.7) by means of the full adiabatic treatment, as described by Born and Huang[5]

$$[\hat{T}_\mathbf{s} + \hat{V}(\mathbf{s},\chi)]\psi_v(\mathbf{s};\chi) = \mathcal{E}_v(\chi)\, \psi_v(\mathbf{s};\chi) \tag{I.9a}$$

$$[\hat{T}_\chi + \mathcal{E}_v(\chi) + \hat{B}_v(\chi)]\Xi^{(A)}_{vm}(\chi) = E^{(A)}_{vm}\Xi^{(A)}_{vm}(\chi) \tag{I.9b}$$

corresponding to the total adiabatic wave function

$$\Psi^{(A)}(\mathbf{s},\chi) = \psi_v(\mathbf{s};\chi)\, \Xi^{(A)}_{vm}(\chi) \tag{I.10}$$

with associated eigenvalue

$$E^{(A)}_{vm} = \langle \Xi^{(A)}_{vm} | \hat{H} | \Xi^{(A)}_{vm} \rangle \tag{I.11}$$

Comparison of (I.9b) with (I.1) shows that the effective torsional potential $\hat{\mathcal{V}}^{(eff)}_v$ is in this case to be identified with

$$\hat{\mathcal{V}}^{(A)}_v(\chi) = \mathcal{E}_v(\chi) + \hat{B}_v(\chi) \tag{I.12}$$

Mills employed such expressions to account for the dependence of low-frequency motions on the high-frequency vibrations of $(HF)_2$, similar to the torsion–vibration dependence considered here. Of course, if the KE-coupling operator $\hat{B}_v(\chi)$ is indeed appreciable, it may be necessary to consider additional terms in a general expansion of the form

$$\Psi^{(NA)}(\mathbf{s},\chi) \simeq \Psi^{(A)}(\mathbf{s},\chi) + \sum_{v',m'} c_{vmv'm'}\Psi_{v'm'}{}^{(A)} \tag{I.13}$$

leading to "curve crossings" among the adiabatic states.

Although attention has largely focused on kinetic energy coupling terms, a recent picture of the electronic origin of internal rotation barriers[10] suggests that potential energy coupling terms in $\hat{V}(\mathbf{s},\chi)$ should lead to an *increase* of the trans barrier with increasing OH excitation. Thus, this picture suggests that PE-coupling terms in $\mathcal{E}_v(\chi)$ may be adequate, both in sign and magnitude, to account for the observed experimental behavior. Since theoretical studies of torsion–vibration interactions in highly excited vibrational states of H_2O_2 were previously unavailable, we undertook to investigate the H_2O_2 potential energy surface $\hat{V}(\mathbf{s},\chi)$ at a high level of ab initio theory in order to determine these PE-coupling effects quantitatively. We have found that PE-coupling effects arising from $\hat{V}(\mathbf{s},\chi)$, evaluated over a suitable local mode vibrational distribution, lead to increases of the H_2O_2 trans barrier with OH overtone excitation which are in good agreement with the experimental results. Thus, the role of KE-coupling terms is apparently rather small in this molecule. Our results thereby provide evidence for the importance of PE-coupling effects of electronic origin, as well as general support for the local mode picture of OH overtone excitations and the general adequacy of the Born–Oppenheimer approximation (I.3)–(I.6) for torsion–vibration interactions in H_2O_2. In the course of this work we have also obtained a refined theoretical equilibrium geometry of hydrogen peroxide, employing basis sets beyond those previously applied to this difficult molecule, and have thereby obtained significantly improved agreement between theory and experiment.

The outline of the paper is as follows: In section II we present a derivation of our procedure, leading to expressions for the evaluation of the v-dependent trans barrier height (h_v) in terms of an accurately known potential energy surface $\hat{V}(\mathbf{s},\chi)$, within the Born–Oppenheimer framework (I.3)–(I.6). Section III describes the ab initio calculations that were carried out in order to evaluate the required points of $\hat{V}(\mathbf{s},\chi)$, leading to the evaluation of h_v and the equilibrium torsional angle χ_v^{eq}, in good agreement with experiment. Section IV discusses possible uncertainties in the calculated values, including effects of basis set limitations and incomplete treatment of electron correlation. Section V presents a final summary and conclusions of our work.

II. Potential Coupling of Torsion and OH Stretch in a Local Mode Picture

Exact evaluation of the trans barrier h_v in the Born–Oppenheimer approximation

$$h_v = \mathcal{E}_v(\pi) - \mathcal{E}_v(\chi_v^{eq}) \tag{II.1}$$

requires exact knowledge of the full six-dimensional potential energy surface $\hat{V}(\mathbf{s},\chi)$ of the vibrational Hamiltonian

$$\hat{H}_\mathbf{s} = \hat{T}_\mathbf{s} + \hat{V}(\mathbf{s},\chi) \tag{II.2}$$

Computation of such a surface is not currently feasible with available ab inito technology. Furthermore, much of the surface is not likely to be of importance for describing the coupling of OH stretches to the torsion, the physical property which is most directly probed in the experimental overtone spectra.

We have therefore chosen to approximate $\mathcal{E}_v(\chi)$ via a variational integral

$$\tilde{\mathcal{E}}_v(\chi) = \langle \tilde{\psi}_v | \hat{H}_\mathbf{s} | \tilde{\psi}_v \rangle_\mathbf{s} \tag{II.3}$$

for a suitable wave function, $\tilde{\psi}_v(\mathbf{s};\chi)$. The variational principle guarantees that first-order deviations in the wave function lead to at most second order errors in $\tilde{\mathcal{E}}_v(\chi)$. The trial wave function $\tilde{\psi}_v(\mathbf{s};\chi)$ will be chosen to represent the salient physical features of the overtone excited state, and this in turn dictates the portions of the potential energy surface $\hat{V}(\mathbf{s},\chi)$ that are needed to evaluate $\tilde{\mathcal{E}}_v(\chi)$ and h_v accurately. This procedure will lead to a feasible strategy for evaluating the quantities that are determined experimentally, *without* the necessity of calculating the full ab initio potential surface. In this section, we outline the steps leading to our final expressions for the trans barrier h_v and equilibrium torsional angle χ_v^{eq} whose evaluation will be described in section III.

A. Choice of the Variational Wave Function. The important *physical* assumptions concerning the nature of the overtone excited states are embodied in the choice of the trial function $\tilde{\psi}_v(\mathbf{s};\chi)$, particularly the description of OH stretching modes which are directly probed in the Dübal–Crim experiment.[4] The overtone states are believed to be most accurately described as *local mode* excitations,[11] corresponding to changes in the bond length R of a single OH bond oscillator. This mode will be represented as a Morse oscillator $\phi_v^{(mo)}(R)$, with parameters[12] chosen to accurately reproduce the experimental vibrational energy levels. In accord with the localized picture of OH excitation, these param-

(8) See, e.g., Sovers, O. J.; Kern, C. W.; Pitzer, R. M.; Karplus, M. *J. Chem. Phys.* **1968**, *49*, 2592–2599. Pitzer, R. M. *Acc. Chem. Res.* **1983**, *16*, 207–210.

(9) Mills, I. M. *J. Phys. Chem.* **1984**, *88*, 532–536.

(10) Brunck, T. K.; Weinhold, F. *J. Am. Chem. Soc.* **1979**, *101*, 1700–1709.

(11) See, e.g., Halonen, L.; Child, M. S. *Mol. Phys.* **1982**, *46*, 239–255.

(12) The empirical Morse potential used to obtain the OH local mode wave functions (eq II.4) is given by the following parameters: $D = 37\,838$ cm^{-1}, $a = 2.317$ Å^{-1} with R_e matched to the MP2-optimized value. We thank Dr. Rolf Dübal for providing the values of these parameters.

TABLE I: Comparison of the v = 0–6 Morse Oscillator Eigenvalues ($\mathcal{E}_v^{(mo)}$) with the Experimental OH Overtone Frequencies[a]

v	$\mathcal{E}_v^{(mo)}$	$\mathcal{E}_v^{(mo)} - \mathcal{E}_0^{(mo)}$	exptl OH overtone freq
0	1876	0	0
1	5486	3610	3605[b]
2	8906	7029	7040[c]
3	12134	10257	10285[c]
4	15174	13294	13350[d]
5	18017	16141	16065[d]
6	20673	18797	18797[d]

[a] All values are given in units of cm^{-1}. Note that the experimental values are not completely unambiguous due to fine structure in the spectra. [b] Text ref 2b. [c] Giguere, P. A. *J. Chem. Phys.* **1950**, *18*, 88. [d] Text ref 4.

eters are chosen to be *independent* of the torsion and other degrees of freedom, so that torsion–vibration coupling effects arise "in first order" through the potential $\hat{V}(\mathbf{s},\chi)$. Since these coupling effects are expected to be small, such a first-order treatment is believed to be well justified and allows the important contributions to the coupling to be isolated and identified conveniently.

The four remaining vibrational coordinates (collectively denoted $\mathbf{s}'$) are considered to play only a secondary role in the interaction of torsion with OH stretch. These will be described by a harmonic oscillator approximation $\phi_0^{(ho)}(\mathbf{s}';\chi)$ of simple product form, with each mode in its vibrational ground state. These secondary coordinates $\mathbf{s}'$ thus make only a "background" zero-point contribution to the torsional properties and can be treated in terms of small-amplitude displacements from their equilibrium values $\mathbf{s}'_{eq}$. However, the frequencies of the secondary modes (unlike that of the local mode R) may be expected to depend somewhat on the torsional angle χ, e.g., through the dependence of $\mathbf{s}'$ G matrix elements on the value of χ.[2a] This effect is incorporated by allowing the function $\phi_0^{(ho)}(\mathbf{s}';\chi)$ to include χ-dependent force constants, calculated from the ab initio surface, which contribute to the torsion–vibration coupling. As we shall see, however, this effect is numerically very small.

In accord with the discussion given above, the vibrational trial function $\tilde{\psi}_v(\mathbf{s};\chi)$ is chosen to be of the form

$$\tilde{\psi}_v(\mathbf{s};\chi) = \phi_v^{(mo)}(R)\phi_0^{(ho)}(\mathbf{s}';\chi) \qquad \text{(II.4)}$$

consisting of an excited-state Morse function and zero-point harmonic oscillator functions for R and $\mathbf{s}'$, respectively. The accuracy of the chosen Morse potential is indicated in Table I, which compares the Morse eigenvalues for v = 0–6 with the experimental vibration frequencies for H_2O_2. The agreement is seen to be very good, suggesting that a trial function of the form (II.4) should provide a satisfactory description of the overtone vibrational properties of H_2O_2.

B. Perturbation Decomposition. The choice (II.4) of the vibrational trial function can be further motivated by rewriting the vibrational Hamiltonian $\hat{H}_s$ as a sum of two operators: (i) a zero-order operator $\hat{H}^{(0)}$, for which $\tilde{\psi}_v(\mathbf{s};\chi)$ is an eigenfunction, and (ii) a remaining coupling operator, $\hat{H}^{(1)}$, which acts as a perturbation. In particular, only the terms appearing in $\hat{H}^{(1)}$ will be able to *directly* couple the OH stretch to the torsion. Since the form of the local-mode OH oscillator wave function is taken to be independent of χ, $\hat{H}^{(0)}$ can only indirectly couple the overtone vibration to the torsion through the χ-dependence of the unexcited normal modes for $\mathbf{s}'$, an effect which is expected to be small.

The approximate wave function $\tilde{\psi}_v(\mathbf{s};\chi)$ satisfies the following zero-order wave equation

$$\hat{H}^{(0)}\tilde{\psi}_v(\mathbf{s};\chi) = \tilde{\mathcal{E}}_v^{(0)}(\chi)\,\tilde{\psi}_v(\mathbf{s};\chi) \qquad \text{(II.5)}$$

The zero-order Hamiltonian $\hat{H}^{(0)} = \hat{H}^{(mo)} + \hat{H}^{(ho)}$ can be written in terms of a Morse oscillator Hamiltonian $\hat{H}^{(mo)}$ for the local OH stretch and a harmonic oscillator Hamiltonian $\hat{H}^{(ho)}$ for the other unexcited modes

$$\hat{H}^{(mo)} = \hat{T}_R + \hat{V}^{(mo)}(R) \qquad \text{(II.6a)}$$

$$\hat{H}^{(ho)} = \hat{T}_{s'} + \tfrac{1}{2}\mathbf{k}'(\chi)(\mathbf{s}' - \mathbf{s}'_{eq})^2 \qquad \text{(II.6b)}$$

In eq II.6a, $\hat{V}^{(mo)}(R)$ represents the local OH Morse potential, with associated Morse eigenvalue $\mathcal{E}_v^{(mo)}$ for overtone state v

$$\hat{H}^{(mo)}\phi_v^{(mo)}(R) = \mathcal{E}_v^{(mo)}\phi_v^{(mo)}(R) \qquad \text{(II.7)}$$

and in eq II.6b, $\mathbf{k}'(\chi)$ denotes a set of χ-dependent harmonic force constants for the secondary modes, leading to a corresponding zero-point eigenvalue $\mathcal{E}_0^{(ho)}(\chi)$ for these modes

$$\hat{H}^{(ho)}\phi_0^{(ho)}(\mathbf{s}';\chi) = \mathcal{E}_0^{(ho)}(\chi)\,\phi_0^{(ho)}(\mathbf{s}';\chi) \qquad \text{(II.8)}$$

We can therefore partition the Hamiltonian as

$$\hat{H}_s = \hat{H}^{(0)} + \hat{H}^{(1)} = \hat{H}^{(mo)} + \hat{H}^{(ho)} + \hat{H}^{(1)} \qquad \text{(II.9)}$$

where

$$\hat{H}^{(0)} = \hat{T}_s + \hat{V}^{(0)}(\mathbf{s},\chi) \qquad \text{(II.10a)}$$

$$\hat{H}^{(1)} = \hat{V}(\mathbf{s},\chi) - \hat{V}^{(0)}(\mathbf{s},\chi) \qquad \text{(II.10b)}$$

and where

$$\hat{V}^{(0)} = \hat{V}^{(0)}(R,\chi,\mathbf{s}') = \hat{V}^{(mo)}(R) + \tfrac{1}{2}\mathbf{k}'(\chi)(\mathbf{s}' - \mathbf{s}'_{eq})^2 \qquad \text{(II.11)}$$

is the potential energy for the zero-order equation (II.5) with eigenvalue

$$\tilde{\mathcal{E}}_v^{(0)}(\chi) = \mathcal{E}_v^{(mo)} + \mathcal{E}_0^{(ho)}(\chi) \qquad \text{(II.12)}$$

The Born–Oppenheimer effective torsional potential then becomes

$$\tilde{\mathcal{E}}_v(\chi) = \tilde{\mathcal{E}}_v^{(0)}(\chi) + \langle\tilde{\psi}_v|\hat{H}^{(1)}|\tilde{\psi}_v\rangle_s \qquad \text{(II.13)}$$

where the dominant contribution to torsion–vibration interaction is contained in the perturbative coupling potential of eq II.10b.

C. Reduction of the Coupling Potential to Two-Dimensional Form. The potential difference of eq II.10b is formally dependent on all six degrees of freedom of the H_2O_2 potential energy surface. However, since this potential difference only occurs in the integral of eq II.13, we can make approximations to $\hat{V}(R,\chi,\mathbf{s}')$ that are consistent with the remaining factor $|\tilde{\psi}_v|^2$ of the integrand. It is this effective averaging of $\hat{H}^{(1)}$ over the zero-order wave function that reduces the amount of information about the full potential $\hat{V}(R,\chi,\mathbf{s}')$ that is required to evaluate $\tilde{\mathcal{E}}_v(\chi)$.

In order to evaluate the integral $\langle\tilde{\psi}_v|\hat{H}^{(1)}|\tilde{\psi}_v\rangle_s$ of eq II.13, we may expand the full potential $\hat{V}(R,\chi,\mathbf{s}')$ in a Taylor series about the equilibrium values $\mathbf{s}'_{eq}$ of the secondary coordinates, leading to an equation of the form

$$\hat{V}(R,\chi,\mathbf{s}') = \hat{V}^{(eq)}(R,\chi) + \tfrac{1}{2}\mathbf{k}'(\chi)(\mathbf{s}' - \mathbf{s}'_{eq})^2 + \ldots \qquad \text{(II.14)}$$

for each R, χ. In this equation, the symbol $\hat{V}^{(eq)}(R,\chi)$ has been introduced to denote the effective *two*-dimensional potential obtained from the full $\hat{V}(R,\chi,\mathbf{s}')$ by "relaxing" the secondary coordinates $\mathbf{s}'$ to their equilibrium values

$$\hat{V}^{(eq)}(R,\chi) \equiv \hat{V}(R,\chi,\mathbf{s}'_{eq}) \qquad \text{(II.15)}$$

for each R, χ. This two-dimension potential will govern the dominant potential coupling between torsion and OH stretch, while also incorporating the leading contributions of couplings to the secondary unexcited modes $\mathbf{s}'$.

We therefore approximate $\hat{V}(R,\chi,\mathbf{s}')$ by truncating the expansion II.14 beyond the terms of second order (consistent with a normal mode picture for the unexcited modes). The coupling potential (II.10b) becomes

$$\hat{H}^{(1)} = \hat{V}^{(eq)}(R,\chi) - \hat{V}^{(mo)}(R) \qquad \text{(II.16)}$$

With this simplification, the perturbative coupling operator no longer depends explicitly on the $\mathbf{s}'$ coordinates. Integration over these variables contributes only a normalization integral, and the second term in (II.13) becomes simply a one-dimensional quadrature over the Morse eigenfunction

$$\tilde{\mathcal{E}}_v(\chi) = \tilde{\mathcal{E}}_v^{(0)}(\chi) + \langle\phi_v^{(mo)}|\hat{V}^{(eq)}(R,\chi) - \hat{V}^{(mo)}(R)|\phi_v^{(mo)}\rangle_R \qquad \text{(II.17)}$$

D. Evaluation of the Trans Barrier. The trans barrier in overtone state v is given by

$$h_v = \tilde{\mathcal{E}}_v(\pi) - \tilde{\mathcal{E}}_v(\chi_v^{eq}) \quad \text{(II.18)}$$

where χ_v^{eq} is the angle at which the effective Born–Oppenheimer torsional potential $\mathcal{E}_v(\chi)$ is minimized

$$\left.\frac{\partial \mathcal{E}_v(\chi)}{\partial \chi}\right|_{\chi_v^{eq}} = 0 \quad \text{(II.19)}$$

From eq II.12 and II.17, the expression for the trans barrier reduces to

$$h_v = \mathcal{E}_0^{(ho)}(\pi) - \mathcal{E}_0^{(ho)}(\chi_v^{eq}) + \langle \phi_v^{(mo)} | \hat{V}^{(eq)}(R,\pi) - \hat{V}^{(eq)}(R,\chi_v^{eq}) | \phi_v^{(mo)} \rangle_R \quad \text{(II.20)}$$

since the local-mode Morse terms depend on R only.

Equation II.20 can also be rewritten in terms of its contributions from the local Morse oscillator mode and the secondary harmonic oscillator modes

$$h_v = h_v^{(mo)} + h_v^{(ho)} \quad \text{(II.21)}$$

with

$$h_v^{(mo)} = \langle \phi_v^{(mo)} | \hat{V}^{(eq)}(R,\pi) - \hat{V}^{(eq)}(R,\chi_v^{eq}) | \phi_v^{(mo)} \rangle_R \quad \text{(II.22a)}$$

$$h_v^{(ho)} = \mathcal{E}_0^{(ho)}(\pi) - \mathcal{E}_0^{(ho)}(\chi_v^{eq}) \quad \text{(II.22b)}$$

The latter term represents the difference in zero-point energies of the harmonic modes, and is expected to be only weakly v-dependent (through χ_v^{eq}). We shall therefore simply neglect the contribution of this term at the present time (its contribution will be estimated in section IV), and proceed with the evaluation of the dominant term

$$h_v \simeq h_v^{(mo)} \quad \text{(II.23)}$$

using eq II.22a.

E. Evaluation of Equilibrium Torsional Angle. One additional approximation will be adopted to reduce eq II.22a to a tractable form. The equilibrium angle χ_v^{eq} defined by eq II.19 would seem to require knowledge of $\tilde{\mathcal{E}}_v(\chi)$ over an extended range of χ, thus necessitating evaluation of $\hat{V}^{(eq)}(R,\chi)$ over an extended two-dimensional region. One might simply introduce the *empirical* value of χ_v^{eq} in order to remove this difficulty, but an alternative procedure will allow us to calculate both χ_v^{eq} and h_v by purely theoretical means.

The simplification is to recognize that $\hat{V}^{(eq)}(R,\chi)$ could be expanded, for any R, as a Taylor series about the equilibrium torsion angle χ_R^{eq} for the fixed value of R

$$\hat{V}^{(eq)}(R,\chi) = \hat{V}^{(eq)}(R,\chi_R^{eq}) + \tfrac{1}{2}k_e(\chi - \chi_R^{eq})^2 + \ldots \quad \text{(II.24)}$$

To a very good approximation, we can therefore replace χ_v^{eq} by the vibrationally averaged value of χ_R^{eq}

$$\chi_v^{eq} \simeq \langle \tilde{\psi}_v | \chi_R^{eq} | \tilde{\psi}_v \rangle_s = \langle \phi_v^{(mo)} | \chi_R^{eq} | \phi_v^{(mo)} \rangle_R \quad \text{(II.25)}$$

the "relaxed" equilibrium torsional angle at each R. The errors implicit in (II.25) are formally of second order, related to the dispersion of χ_R^{eq} values in overtone state v,

$$\delta\chi_R^{eq} = [\langle \phi_v^{(mo)} | (\chi_R^{eq})^2 | \phi_v^{(mo)} \rangle_R - \langle \phi_v^{(mo)} | \chi_R^{eq} | \phi_v^{(mo)} \rangle_R^2]^{1/2} \quad \text{(II.26)}$$

and will eventually be assessed by direct comparison with the experimental value of χ_v^{eq}. The order of error is further reduced when (II.25) is substituted into the right-hand side of (II.24) to evaluate $\hat{V}^{(eq)}(R,\chi_v^{eq})$.

When the approximation II.25 is introduced into eq II.22a [via the formal Taylor series (II.24)], the expression for the trans barrier reduces to

$$h_v = \langle \phi_v^{(mo)} | h(R) | \phi_v^{(mo)} \rangle_R \quad \text{(II.27)}$$

where $h(R)$ is the R-dependent trans barrier

$$h(R) \equiv \hat{V}^{(eq)}(R,\pi) - \hat{V}^{(eq)}(R,\chi_R^{eq}) \quad \text{(II.28)}$$

In effect, these expressions allow h_v to be reduced to a vibrational average over the difference of two *one*-dimensional slices through the six-dimensional potential energy surface [$\hat{V}^{(eq)}(R,\pi)$, $\hat{V}^{(eq)}(R,\chi_R^{eq})$], each of which is feasible to compute by contemporary ab initio electronic structure methods. Equations II.27 and II.28 form the basis for the numerical calculations to be described in the next section.

TABLE II: Summary of Representative Examples of Previous ab Initio Calculations of H_2O_2. Optimized Geometrical Parameters (Bond Lengths R_{OO} and R_{OH}, OOH Bond Angle α_{OOH}, and the Torsional Angle, χ) and the Height of the Trans Barrier h

method/basis set	R_{OO}, Å	R_{OH}, Å	α_{OOH}, deg	χ, deg	h, cm^{-1}
RHF/STO-3G[a]	1.396	1.001	101.12	125.0	25[b]
RHF/[4s2p/2s][c]	1.487	0.972	99.4	180.0	0
RHF/[4s3p1d/2s1p][d]	1.393	0.946	102.5	113.7	384
RHF/(11s6p2d/2s1p)[e]	1.390	0.943	102.9	111.2	504
MP2/[3s2p1d/2s][e]	1.468	0.976	98.8	119.4	210
GVB+CI/SV-DZP[f]	1.464	0.967	99.9	119.1	350
experiment[g]	1.464	0.965	99.44	111.83	385

[a] Newton, M. D.; Lathan, W. A.; Hehre, W. J.; Pople, J. A. *J. Chem. Phys.* **1970**, *52*, 4064. [b] Newton et al. do not report a value for the trans barrier. The value recorded here was found by reproducing their calculations. [c] Ranck, J. P.; Johansen, H. *Theor. Chim. Acta* **1972**, *24*, 334. [d] Text ref 15. [e] Text ref 16. [f] Text ref 17. [g] Text ref 14.

III. Ab Initio Computations of $h(R)$ and χ_R^{eq}

A. Equilibrium Geometry and Trans Barrier. Previous computational work on H_2O_2 has found that both the predicted equilibrium geometry and the height of the trans barrier are sensitive functions of the size and composition of the basis set and the degree of electron correlation in the method. Table II presents a summary of the computed equilibrium geometry and trans barrier found by representative examples of the earlier work as well as the current experimental values.

It should be noted that there is considerable confusion in the literature concerning the correct experimental *equilibrium* geometry of H_2O_2. The major source of conflict is the value of the equilibrium torsional angle χ_{eq}. On one side, most ab initio calculations (see Table II) and a microwave study done by Khachkuruzov and Przhevalskii[13] find χ_{eq} to be about 120°, while on the other side, Hunt and co-workers[2c] conclude on the basis of an infrared study that χ_{eq} is closer to 110° (111.5°). Recently, Koput[14] argued strongly on behalf of a value of 111.83° for the equilibrium torsional angle, showing that the value of 119.1° given by Khachkuruzov and Przhevalskii corresponds to the *average* equilibrium torsional angle, which is computed by averaging the torsional angle over the torsional wave function. Whenever we refer to the experimental geometry of H_2O_2, we are referring to the values recommended by Koput.

Of the early SCF calculations, the most comprehensive study was performed by Dunning and Winter.[15] They confirmed that including polarization functions in the basis set was essential to obtain a non-zero trans barrier. Furthermore, their study indicated that it is necessary to optimize the other geometrical parameters for each torsional angle in order to compute an accurate torsional potential. Their computed trans barrier is in excellent agreement with the experimental value, but the predicted equilibrium geometry differs significantly from the experimental values. In particular, the O–O bond length is predicted to be too short by about 0.07 Å (1.392 vs 1.464 Å) and the OOH bond angle is too large by three degrees (102.5° vs 99.4°). Their computed torsional angle is in fair agreement with experiment (113.7° vs 111.8°).

Later work by Cremer[16] and by Bair and Goddard[17] indicates that the discrepancy with experiment found by Dunning and Winter for the O–O bond length and OOH bond angle is due to a lack of electron correlation in the SCF method. Whereas Cremer

(13) Khachkuruzov, G. A.; Przhevalskii, I. N. *Opt. Spectrosc.* **1974**, *36*, 172–174.
(14) Koput, J. *J. Mol. Spectrosc.* **1986**, *115*, 438–441.
(15) Dunning, Jr., T. H.; Winter, N. W. *J. Chem. Phys.* **1975**, *63*, 1847–1855.
(16) Cremer, D. *J. Chem. Phys.* **1978**, *69*, 4440–4455.
(17) Bair, R. A.; Goddard, III, W. A. *J. Am. Chem. Soc.* **1982**, *104*, 2719–2724.

TABLE III: Equilibrium Geometry and Trans Barrier Computed with the MP2 Method at Various Basis Set Levels[a]

method/basis set	R_{OO}, Å	R_{OH}, Å	α_{OOH}, deg	χ, deg	h, cm^{-1}
MP2/6-31G*	1.468	0.976	98.8	119.4	210
MP2/6-311G(2d,p)	1.455	0.965	99.1	116.0	312
MP2/6-311G(3d,2p)	1.450	0.962	99.5	111.1	448

[a] Table II lists the results of previous calculations and the current experimental values.

found significant improvement in the two geometrical parameters at the MP2 (second-order Møller–Plesset perturbation theory) level,[18,19] his computed trans barrier is too low by 174 cm^{-1}. Both studies predict that the equilibrium torsional angle is approximately 120°, in disagreement with the best experimental value. In general, the fair agreement with experiment obtained at the SCF level by Dunning and Winter is unstable with respect to inclusion of correlation or expansion of the basis set.

Our calculations start at the MP2/6-31G* level.[18-20] Based upon previous work, this is the minimum level needed to obtain reasonable agreement with experiment. MP2, as opposed to simple SCF theory, is necessary to obtain an accurate geometry, particularly the O–O bond length. Polarization functions are necessary to obtain a nonzero value for the trans barrier. Because this research is primarily concerned with computing the trans barrier, we also performed full geometry optimizations at the MP2 level with two larger basis sets,[20] 6-311G(2d,p) and 6-311G(3d,2p), to assess the sensitivity of the computed geometry and trans barrier to basis set enhancement. Both basis sets are of split-valent triple zeta quality in the sp portion and contain multiple polarization functions, significantly beyond what has previously been applied to this molecule. All MP2 computations reported here were performed with the ab initio program GAUSSIAN 82.[21] Table III presents the equilibrium geometry and trans barrier computed at these basis set levels.

It is apparent that the addition of more polarization functions has a large effect on both the equilibrium geometry and the trans barrier. The equilibrium torsional angle decreases from about 120° at the MP2/6-31G* level to 111.1° at the MP2/6-311G-(3d,2p) level, in much better agreement with experiment (see Table II). However, at the largest basis set level, the computed O–O bond length (R_{OO}) is too short by about 0.016 Å. Reflecting the short R_{OO} value, the computed trans barrier is too high by 63 cm^{-1}. We conjecture that both of these discrepancies are due to incomplete treatment of correlation and that more accurate values could be obtained with a more highly correlated method[22] at the 6-311G(3d,2p) level. However, the MP2/6-311G(3d,2p) treatment provides a reasonably accurate description that should be adequate for the present purpose.

B. Trans Barrier for Stretched Values of the OH Bond. At stretched values of the local OH bond length R, the trans barrier $h(R)$ can be computed (eq II.28) by optimizing the s′ coordinates and χ to obtain $\mathcal{V}_e(R,\chi_R^{eq})$ (and χ_R^{eq}), then repeating the computation with the molecule fixed in the trans conformation ($\chi = \pi$) to obtain $\mathcal{V}_e(R,\pi)$. Accurate evaluation of the vibrationally averaged trans barrier requires knowledge of $h(R)$ over the range of R where the Morse oscillator wave functions have significant amplitude. Table IV gives the value of the normalization integral[23] for the $v = 0$–8 Morse oscillator wave functions when integrated from $R = 0.50$ to 1.80 Å. It is clear from the values given that integration over this finite range is sufficient to pick up over 99% of the vibrational density for the first nine Morse oscillator states. We have therefore sought to evaluate $h(R)$ over the range 0.5 Å $\leq R \leq$ 1.8 Å, in order to carry out the vibrational averaging (eq II.27) with sufficient accuracy for overtone states up to $v = 8$.

TABLE IV: Integral of the $v = 0$–8 Morse Oscillator Vibrational Densities over the Region of R between 0.5 and 1.8 Å Computed by Quadrature[a]

v	$N(0.5,1.8)$	v	$N(0.5,1.8)$	v	$N(0.5,1.8)$
0	1.000 00	3	1.000 00	6	0.999 98
1	1.000 00	4	1.000 00	7	0.999 49
2	1.000 00	5	1.000 00	8	0.991 76

[a] The integral, $N(a,b)$, is defined by

$$N(a,b) = \int_a^b |\phi_v^{(mo)}|^2 \, dR$$

where $N(0,\infty) = 1$.

TABLE V: Optimized Geometrical Parameters, Total Energies, and Trans Barrier Heights of H_2O_2 as a Function of the Local OH Stretch R Computed at the MP2/6-31G* Level

		s′ coordinates					
R	χ	R_{OO}	R_{OH}	α	α_{OOH}	total energy	$h(R)$
0.50	116.90	1.4253	0.9751	100.29	100.18	−150.324 893 8	391
	180.0	1.4368	0.9735	99.62	98.58	−150.323 117 4	
0.60	119.03	1.4399	0.9751	99.58	99.71	−150.775 732 6	322
	180.0	1.4491	0.9737	98.96	98.32	−150.774 265 1	
0.70	121.06	1.4507	0.9751	99.18	99.36	−150.993 685 9	263
	180.0	1.4600	0.9741	98.38	97.96	−150.992 486 7	
0.80	122.06	1.4592	0.9752	98.88	99.02	−151.091 862 4	221
	180.0	1.4679	0.9744	97.98	97.67	−151.090 847 0	
0.90	121.85	1.4651	0.9754	98.72	98.80	−151.128 783 6	206
	180.0	1.4746	0.9748	97.56	97.40	−151.127 845 7	
R_{eq}	119.38	1.4676	0.9756	98.77	98.77	−151.134 914 9	210
	180.0	1.4788	0.9752	97.20	97.20	−151.133 956 9	
1.00	118.50	1.4680	0.9757	98.80	98.75	−151.134 409 3	216
	180.0	1.4802	0.9752	97.15	97.19	−151.133 426 9	
1.05	117.00	1.4686	0.9758	98.88	98.70	−151.130 741 7	234
	180.0	1.4802	0.9754	97.00	97.00	−151.129 674 6	
1.10	115.50	1.4692	0.9760	98.97	98.70	−151.124 468 1	263
	180.0	1.4836	0.9757	96.68	96.96	−151.123 270 9	
1.15	113.53	1.4681	0.9761	99.31	98.84	−151.116 464 3	305
	180.0	1.4847	0.9759	96.50	96.90	−151.115 076 8	
1.20	111.48	1.4664	0.9764	99.61	98.93	−151.107 376 2	361
	180.0	1.4859	0.9762	96.36	96.83	−151.105 729 6	
1.25	109.48	1.6644	0.9754	99.95	99.02	−151.097 684 9	436
	180.0	1.4870	0.9764	96.25	96.75	−151.095 699 2	

[a] Equilibrium and trans conformations are given for each value of R. Bond lengths (R, R_{OO}, R_{OH}) are given in units of Å; bond angles (α, α_{OOH}) and the torsional angle (χ) are given in units of degrees; total energies are given in atomic units, and the trans barrier height ($h(R)$) is given in units of cm^{-1}. The unsubscripted geometrical parameters (R and α) describe the geometry of the dissociative OH group.

For R between 0.5 and 1.25 Å, the geometry optimizations required to evaluate $h(R)$ were performed at the MP2/6-31G* level. Table V gives the optimized geometries, total energies, and trans barrier heights obtained in this way. In light of our results on the equilibrium trans barrier, the computed $h(R)$ values were refined by recalculating each point with the two larger basis sets, 6-311G(2d,p) and 6-311G(3d,2p), using the 6-31G* geometries. Table VI gives the total energies and trans barrier heights obtained at these higher basis set levels. Ideally, the geometry would be reoptimized for each value of R at each of the two larger basis set levels, but such a procedure is computationally quite expensive. The error introduced by not reoptimizing the geometries was

(18) Møller, C.; Plesset, M. S. *Phys. Rev.* **1934**, *46*, 618–622.
(19) Pople, J. A.; Binkley, J. S.; Seeger, R. *Int. J. Quantum Chem.* **1976**, *S10*, 1–19.
(20) 6-31G*: Hehre, W. J.; Ditchfield, R.; Pople, J. A. *J. Chem. Phys.* **1972**, *56*, 2257–2261. Hariharan, P. C.; Pople, J. A. *Theor. Chim. Acta* **1973**, *28*, 213–222. 6-311G: Krishnan, R.; Binkley, J. S.; Seeger, R.; Pople, J. A. *J. Chem. Phys.* **1980**, *72*, 650–654. "++" diffuse functions: Clark, T.; Chandrasekhar, J.; Spitznagel, G. W.; Schleyer, P. v. R. *J. Comput. Chem.* **1983**, *4*, 294–301. (df,p) supplementary functions: Frisch, M. J.; Pople, J. A.; Binkley, J. S. *J. Chem. Phys.* **1984**, *80*, 3265–3269.
(21) All calculations were carried with VAX (revision H) and CRAY CTSS (revision K) versions of GAUSSIAN 82. This program was developed by J. S. Binkley, M. J. Frisch, D. J. Defrees, K. Ravhavachri, R. A. Whiteside, H. B. Schlegel, E. M. Fluder, and J. A. Pople (Carnegie-Mellon University, Pittsburgh, PA).
(22) Bair and Goddard (ref 17) obtained an accurate value of R_{OO} using a CI wave function built from single, double and selected quadruple excitations out of a GVB reference state.
(23) Numerical integrations were carried out by a Romberg integration method (see Press, W. H.; Flannery, B. P.; Teukolsky, S. A.; Vetterling, W. T. *Numerical Recipes: The Art of Scientific Computing*; Cambridge University Press; Cambridge, U. K., 1986, Chapter 4) to an accuracy of 10^{-7}.

TABLE VI: Total Energies and Trans Barrier $h(R)$ of H_2O_2 as a Function of the Local OH Stretch R Computed at the MP2/6-311G(2d,p) and MP2/6-311G(3d,2p) Levels for the MP2/6-31G* Optimized Geometries (see Table V)

		total energy, au		$h(R)$, cm^{-1}	
R	χ	(2d,p)	(3d,2p)	(2d,p)	(3d,2p)
0.50	116.90	−150.489 223 8	−150.509 154 3	433	512
	180.0	−150.487 250 6	−150.506 822 2		
0.60	119.03	−150.926 774 4	−150.943 073 5	369	475
	180.0	−150.925 091 5	−150.940 910 1		
0.70	121.06	−151.134 588 4	−151.149 115 3	327	451
	180.0	−151.133 097 2	−151.147 058 8		
0.80	122.06	−151.227 544 1	−151.240 790 8	294	411
	180.0	−151.226 204 8	−151.238 918 5		
0.90	121.85	−151.261 662 1	−151.273 871 5	296	416
	180.0	−151.260 312 5	−151.271 976 3		
R_{eq}	119.38	−151.266 366 2	−151.278 003 2	312	438
	180.0	−151.264 946 6	−151.276 008 6		
1.00	118.50	−151.265 462 6	−151.276 953 9	322	450
	180.0	−151.263 997 2	−151.274 904 2		
1.05	117.00	−151.261 028 7	−151.272 268 1	342	472
	180.0	−151.259 470 4	−151.270 116 6		
1.10	115.50	−151.254 039 1	−151.265 084 6	369	500
	180.0	−151.252 357 3	−151.262 806 4		
1.15	113.53	−151.245 393 2	−151.256 323 8	413	551
	180.0	−151.243 510 6	−151.253 814 4		
1.20	111.48	−151.235 687 4	−151.246 518 6	469	609
	180.0	−151.233 551 8	−151.243 745 3		
1.25	109.48	−151.225 410 7	−151.236 168 1	540	681
	180.0	−151.222 950 8	−151.233 063 8		

TABLE VII: Optimized Geometrical Parameters, Total Energies, and Trans Barrier Heights of H_2O_2 as a Function of the Local OH Stretch R Computed at the MP2/6-311G(2d,p) and MP2/6-311G(3d,2p) Levels[a]

		s' coordinates					
R	χ	R_{OO}	R_{OH}	α	α_{OOH}	total energy	$h(R)$
				MP2/6-311G(2d,p)			
0.50	115.59	1.4189	0.9652	99.75	100.35	−150.531 462 3	434
	180.0	1.4285	0.9637	99.29	98.88	−150.529 486 1	
0.80	118.11	1.4463	0.9652	99.31	99.38	−151.269 403 6	312
	180.0	1.4547	0.9642	98.42	98.05	−151.268 014 9	
R_{eq}	116.03	1.4550	0.9650	99.07	99.07	−151.307 980 8	312
	180.0	1.4651	0.9646	97.61	97.61	−151.306 557 2	
1.20	108.43	1.4540	0.9660	99.84	99.17	−151.276 972 2	477
	180.0	1.4744	0.9656	96.52	97.09	−151.274 800 2	
				MP2/6-311G(3d,2p)			
0.50	113.95	1.4147	0.9611	99.98	100.69	−150.555 516 0	508
	180.0	1.4244	0.9595	99.40	99.20	−150.553 201 5	
0.80	114.00	1.4414	0.9614	99.79	99.73	−151.286 229 0	444
	180.0	1.4498	0.9601	98.89	98.44	−151.284 206 7	
R_{eq}	111.08	1.4500	0.9620	99.49	99.49	−151.232 161 7	449
	180.0	1.4601	0.9608	98.04	98.04	−151.321 116 3	
1.20	104.02	1.4500	0.9620	100.10	99.61	−151.291 216 1	626
	180.0	1.4697	0.9619	96.80	97.50	−151.288 361 7	

[a] Equilibrium and trans conformations are given for each value of R. Bond lengths (R, R_{OO}, R_{OH}) are given in units of Å; bond angles (α, α_{OOH}) and the torsional angle (χ) are given in units of degrees; total energies are given in atomic units, and the trans barrier height $h(R)$ is given in units of cm^{-1}.

investigated for selected values of R. Table VII gives the details of these optimizations for R = 0.5 and 0.8 Å, R_{eq}, and 1.20 Å. Comparison of the trans barrier heights found at the higher basis set levels with (Table VII) and without (Table VI) geometry optimization indicates that the error in $h(R)$ due to not reoptimizing the geometry is less than 35 cm^{-1}. Figure 1a,b shows the calculated $h(R)$ and χ_R^{eq} values generated at the MP2 level for R between 0.5 and 1.2 Å.

Figure 1a clearly shows that the trans barrier $h(R)$ increases as R is stretched, as well as when R is compressed. Figure 1b shows that the equilibrium torsional angle χ_R^{eq} is also strongly dependent upon the value of R. Both parts of Figure 1 show that although the magnitude of the $h(R)$ and χ_R^{eq} curves is dependent upon the basis set used, the shape of the curves is rather less

TABLE VIII: Optimized Geometrical Parameters, Total Energies, and Trans Barrier Heights of H_2O_2 as a Function of the Local OH Stretch R Computed at the GVB/6-31G* Level[a]

		s' coordinates					
R	χ	R_{OO}	R_{OH}	α	β	total energy	$h(R)$
0.50	118.75	1.4486	0.9691	99.55	100.01	−150.081 814 4	333
	180.0	1.4615	0.9678	98.98	98.67	−150.080 298 3	
0.75	125.83	1.4851	0.9690	98.54	98.93	−150.809 702 7	187
	180.0	1.4955	0.9683	97.86	97.88	−150.808 851 8	
R_{eq}	124.69	1.4994	0.9693	98.49	98.49	−150.887 668 1	156
	180.0	1.5114	0.9688	97.36	97.36	−150.886 955 7	
1.20	115.77	1.4976	0.9699	99.13	98.66	−150.859 560 8	309
	180.0	1.5183	0.9697	96.93	97.11	−150.858 152 4	
1.50	101.13	1.4708	0.9708	100.95	99.82	−150.808 340 2	979
	180.0	1.5159	0.9711	96.72	97.10	−150.803 881 4	
1.80	91.50	1.4330	0.9712	103.35	101.29	−150.776 860 7	1971
	180.0	1.5023	0.9720	97.05	97.49	−150.767 882 4	
2.10	90.08	1.4071	0.9716	105.35	102.02	−150.762 503 8	2733
	180.0	1.4863	0.9719	106.76	102.40	−150.750 052 2	
2.40	90.13	1.3956	0.9718	106.76	102.40	−150.756 939 2	1638
	180.0	1.3878	0.9719	99.63	102.64	−150.749 474 7	
2.70	90.20	1.3911	0.9719	107.99	102.51	−150.754 901 8	612
	180.0	1.3881	0.9719	103.88	102.65	−150.752 113 4	

[a] Equilibrium and trans conformations are given for each value of R. Bond lengths (R, R_{OO}, R_{OH}) are given in units of Å; bond angles (α, β) and the torsional angle (χ) are given in units of degrees; total energies are given in atomic units, and the trans barrier height ($h(R)$) is given in units of cm^{-1}.

TABLE IX: Total Energies (in au) and Trans Barrier $h(R)$ (in cm^{-1}) of H_2O_2 as a Function of the Local OH Stretch R Computed at the GVB/6-311G(2d,p) Level for the GVB/6-31G* Optimized Geometries (see Table VIII)

		GVB/6-311G(2d,p)	
R	χ	total energy	$h(R)$
R_{eq}	124.69	−150.938 164 1	233
	180.0	−150.937 102 6	
1.20	115.77	−150.908 759 7	404
	180.0	−150.906 919 2	
1.50	101.13	−150.855 909 1	1076
	180.0	−150.851 008 4	
1.80	91.50	−150.823 630 3	2060
	180.0	−150.814 244 5	

sensitive to changes in the basis.

For R beyond 1.25 Å, the OH bond starts to dissociate (HOOH → HOO• + H•), and the closed-shell RHF reference wave function becomes inadequate to describe the resulting open-shell singlet diradical state. Therefore, for $R > 1.20$ Å, we used a GVB-PP (generalized valence bond) wave function[24] which is capable of describing the lower energy singlet diradical state. At each basis set level, the GVB wave function consisted of two core orbitals and seven pairs; each bond was paired with its antibond, and each oxygen lone pair was paired with a diffuse Rydberg orbital on the same center. All GVB calculations were performed with the ab initio program GAMESS.[25] GVB/6-31G* results were obtained for values of R out to 2.7 Å. Optimized geometries, total energies, and trans barrier heights obtained at the GVB/6-31G* level are given in Table VIII. Although the v = 0–8 vibrational wave functions do not extend significantly beyond R = 1.8 Å, a larger span of GVB/6-31G* values was investigated in order to establish the long-range behavior of $h(R)$ and to verify that $h(R)$ and χ_R^{eq} approach the expected asymptotic values $h(R) \to 0$, $\chi_R^{eq} \to 90°$ at large R. GVB values for $h(R)$ were also obtained for several values of $R < 1.2$ Å in order to facilitate comparison with

(24) Bobrowicz, F. W.; Goddard, III, W. A. In *Methods of Electronic Structure Theory*; Schaefer, H. F., Ed.; Plenum: New York, 1977; Vol. 2, pp 79–127.

(25) The program GAMESS is originally due to M. Dupuis, D. Spangler, J. J. Wendolski, NRCC Software Catalog, Vol. 1, Program GG01, 1980. The version we used had been heavily modified by M. Schmidt at North Dakota State and S. T. Elbert at Iowa State. We thank Dr. Mike Schmidt and Prof. M. Gordon for providing us with this program.

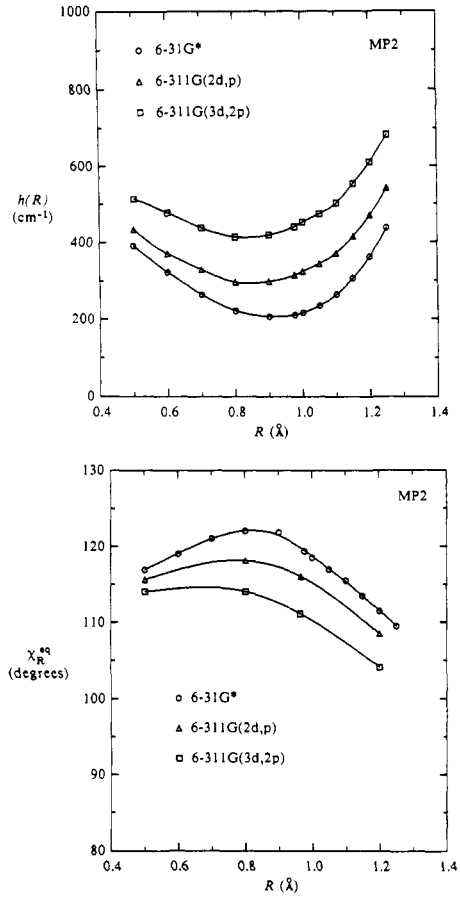

Figure 1. (a, top) Change in the trans barrier, $h(R)$, in H_2O_2 as a function of the local OH stretching coordinate R computed at the MP2 level with three basis sets, 6-31G*, 6-311G(2d,p), and 6-311G(3d,2p). (b, bottom) Change in the optimum torsional angle, χ_R^{eq}, as a function of the local OH stretching coordinate R computed at the MP2 level with three basis sets, 6-31G*, 6-311G(2d,p), and 6-311G(3d,2p).

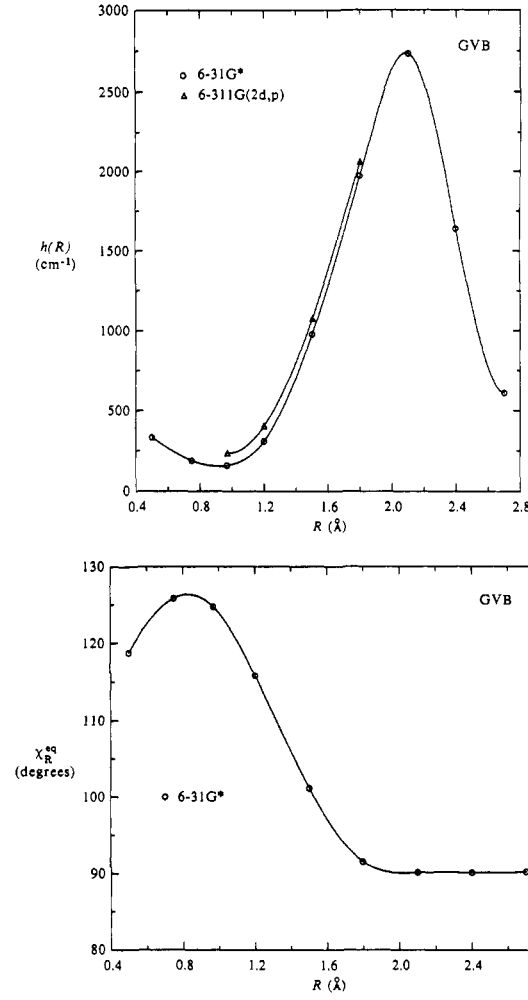

Figure 2. (a, top) Change in the trans barrier, $h(R)$, in H_2O_2 as a function of the local OH stretching coordinate R computed at the GVB level with two basis sets, 6-31G* and 6-311G(2d,p). (b, bottom) Change in the optimum torsional angle, χ_R^{eq}, as a function of the local OH stretching coordinate R computed at the GVB/6-31G* level.

the MP2 results. Computations with the GVB method at larger basis set levels proved to be computationally very expensive due to slow SCF convergence. Hence, only calculations up to the 6-311G(2d,p) basis were possible, and these were performed at four points only, R = 0.9693 Å (R_{eq}), 1.20, 1.50, 1.80 Å. Table IX gives the total energies and trans barrier heights obtained by these GVB/6-311G(2d,p) computations. Geometry optimization at the 6-311G(2d,p) basis set level was not considered feasible and so there is no direct way to assess the error made by not reoptimizing the geometry. However, we expect on the basis of the general similarity of GVB and MP2 results in the region of overlapping R that the error would be less than 50 cm^{-1}.

Figure 2a,b shows the trans barrier $h(R)$ and equilibrium torsional angle χ_R^{eq} curves obtained at the GVB level. Like the MP2 results, $h(R)$ computed by the GVB method increases as R is stretched, rising to almost 2750 cm^{-1} (~8.0 kcal/mol, roughly 8 times the barrier at equilibrium) near R = 2.0 Å before falling toward zero as the O–H bond is stretched to the point of complete dissociation. Similar to the MP2 curves, the 6-311G(2d,p) $h(R)$ curve is greater in magnitude than the 6-31G* curve, but has almost exactly the same R dependence. GVB/6-31G* values for χ_R^{eq} decrease with increasing R, eventually approaching an asymptote of 90°. This value is dictated by the orientation of the pure p-type radical orbital in the peroxy radical, perpendicular to the HOO plane. The long-range dissociative (or reactive) path of the H atom would be along the direction of the radical orbital.

Figure 3a shows the MP2 and GVB $h(R)$ curves drawn over the region of R relevant to the v = 0–8 overtone states (0.5–1.8 Å). It is clear from the figure that both methods at all three basis set levels produce $h(R)$ curves that have the same general shape but differ in magnitude. Moreover, the change in $h(R)$ at a given R upon enlarging the basis set is approximately the same for both methods. For example, at R = 1.2 Å, the difference between the 6-31G* and 6-311G(2d,p) trans barriers is 108 cm^{-1} by the MP2 method and 95 cm^{-1} by the GVB method.

Figure 3b shows corresponding MP2 and GVB χ_R^{eq} curves. To a lesser extent than the $h(R)$ curves (particularly for small R), the shape of the computed χ_R^{eq} curves is approximately the same in both methods and at the three basis set levels.

It is clear from the results of all these calculations (Figures 1–3) that the shape of the torsional potential is strongly dependent upon the local OH stretching motion via pure potential energy coupling effects alone. While the overall magnitude of $h(R)$ and χ_R^{eq} is fairly sensitive to basis set level, the general shape of the respective curves is seen to be quite consistent at all levels of theory considered. The next step is to appropriately average the $h(R)$ and χ_R^{eq} curves over the local OH overtone vibration (modeled by a Morse oscillator) to obtain h_v and χ_v^{eq}.

C. Computation of h_v and χ_v^{eq}. In order to evaluate the integrals defining h_v (eq II.27) and χ_v^{eq} (eq II.25) *continuous* $h(R)$ and χ_R^{eq} curves are needed. We used the observed similarity of the $h(R)$ and χ_R^{eq} curves produced by both MP2 (short-range R) and GVB (long-range R) method to construct continuous curves over the range of R from 0.5 to 1.8 Å.

For $h(R)$, this construction was accomplished by shifting the GVB curves upwards until they match with the MP2 curves at R = 1.2 Å. The combined set of MP2 points and shifted GVB points make up the requisite continuous $h(R)$ curves. One further assumption is needed in order to obtain the $h(R)$ curve for the largest 6-311G(3d,2p) basis set since no GVB points were calculated at that level. Taking into account the observation (section

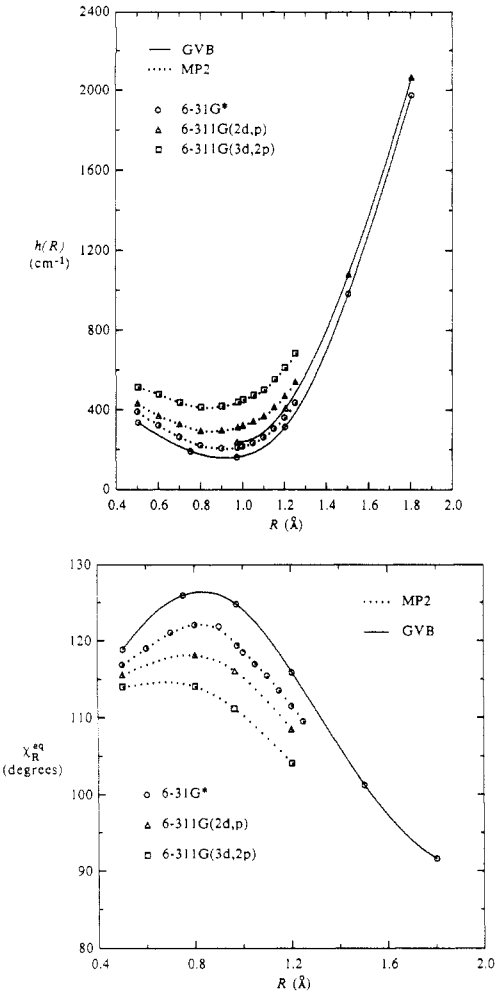

Figure 3. (a, top) Change in the trans barrier, $h(R)$, in H_2O_2 over the region of R relevant to the $v = 0$–6 OH overtone states. Values are given for both MP2 and GVB methods at three basis set levels, 6-31G*, 6-311G(2d,p), and 6-311G(3d,2p). (b, bottom) Equilibrium torsional angle χ_R^{eq} in H_2O_2 as a function of the local OH stretching coordinate R over the range relevant to the $v = 0$–6 OH overtone states. Values are given for two methods, MP2 and GVB, at three basis set levels, 6-31G*, 6-311G(2d,p), and 6-311G(3d,2p).

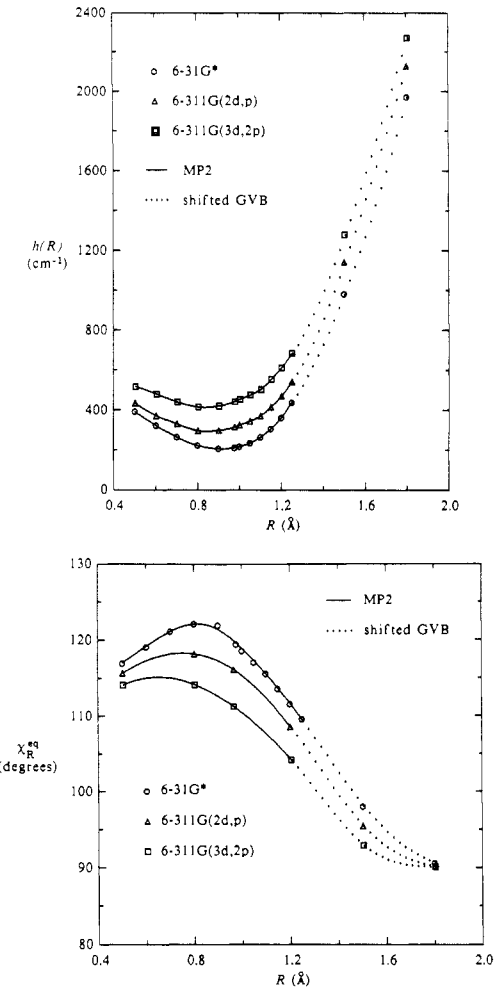

Figure 4. (a, top) Change in the trans barrier, $h(R)$, in H_2O_2 as a function of the local OH stretching coordinate R generated from the MP2 and GVB curves shown in Figure 3a (see text). (b, bottom) Change in the optimum torsional angle, χ_R^{eq}, as a function of the local OH stretching coordinate R over the range relevant to the $v = 0$–6 OH overtone states. The GVB/6-31G* χ_R^{eq} curve (Figures 2b and 3b) was shifted to the end points of the MP2 curves (Figures 1b and 3b) in order to obtain continuous χ_R^{eq} curves (see text). The lines running through the points were obtained by cubic spline interpolation.

III.B) that the change in the trans barrier $h(R)$ with basis set enlargement is approximately the same in the two computational methods, we assumed that the GVB/6-311G(3d,2p) $h(R)$ curve would be shifted upwards from the GVB/6-311G(2d,p) $h(R)$ curve by the same amount (140 cm^{-1}) that the MP2 6-311G(3d,2p) and 6-311G(2d,p) curves differ. Figure 4a shows the final $h(R)$ curves obtained by combining the short-range MP2 results with the long-range GVB results in the manner just described. Cubic spline interpolation[26] was used to generate the smooth lines running through the computed points.

Combining the MP2 and GVB curves to obtain continuous approximations of the equilibrium torsional angle χ_R^{eq} curves is more ambiguous than in the $h(R)$ treatment. This is due mainly to the lack of GVB optimized geometries at the higher basis set levels, so that long-range information about χ_R^{eq} is available only from the GVB/6-31G* points. Simply shifting the GVB curve to match at a single point with MP2 curve is also more suspect in this case, due to larger differences in the shape of the various χ_R^{eq} curves than in the $h(R)$ case. On the other hand, all of the computed χ_R^{eq} curves must approach 90° asymptotically, making the extrapolation of the MP2 results to the long-range GVB region less arbitrary than it might be. Figure 4b shows the set of continuous χ_R^{eq} curves formed by sliding the GVB/6-31G* curve horizontally toward shorter R until the curve matches the MP2 value at $R = 1.2$ Å. A cubic smoothing spline[27] was applied to the 6-31G* set of MP2 and shifted GVB points to generate the 6-31G* line. Regular interpolatory cubic splines[26] were used to generate the 6-311G(2d,p) and 6-311G(3d,2p) lines. Clearly, the joining and smoothing procedures introduce a degree of arbitrariness at larger R that may have appreciable effects in higher vibrational states. Errors produced by such procedures will be discussed more fully in section IV.

Once continuous $h(R)$ and χ_R^{eq} curves have been obtained, it is straightforward to numerically evaluate the integrals for the trans barrier h_v (eq II.27) and the equilibrium torsional angle χ_v^{eq} (eq II.25) by quadrature.[23] Figure 5a,b shows the computed h_v and χ_v^{eq} for $v = 0$–8, and compares those with the available experimental values reported by Dübal and Crim.[4] The figures clearly show that the computed values at all three basis set levels parallel the experimental values and that the largest 6-311G(3d,2p)

(26) We used the IMSL spline interpolation routine ICSCCU which generates a natural cubic spline. For information on natural splines, see Cox, M. G. In *The State of the Art in Numerical Analysis*; Jacobs, D., Ed.; Academic: London, 1977; pp 627–688.

(27) The smoothing spline is necessary due to the great difficulty in obtaining stable values of χ when the associated gradient becomes extremely small, corresponding to the low frequency of the torsional motion in H_2O_2. The gradient of the energy when χ_R^{eq} is within about 0.5° of the real minimum satisfies the normal GAUSSIAN 82 optimization criteria leading to fluctuations in the final χ_R^{eq} value depending upon the closeness of the initial guess to the actual minimum. Note that, because of the low frequency of the torsion, the effect on the total energy of slight errors in the torsional angle is very small.

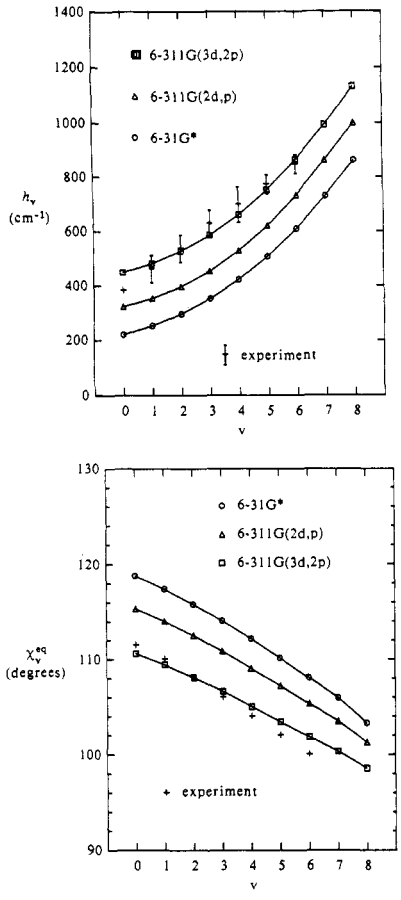

Figure 5. (a, top) Trans barrier height h_v for OH stretching overtones in H_2O_2. Theoretical values (arbitrarily connected by straight lines) are shown for three basis sets. Experimental values are quoted from ref 4. (b, bottom) Calculated equilibrium torsional angle χ_v^{eq} for the OH stretching overtones in H_2O_2. Experimental values were taken from ref 4.

basis provides good (although not perfect) agreement with experiment. The computed h_v curve suggests a slight amount of curvature that does not seem to be present in the experimental values, and the best χ_v^{eq} curve differs from experiment at the highest values of v by as much as 1–2°. In the next section, we will estimate more fully the errors in the computed h_v and χ_v^{eq} curves. However, the good agreement with experiment shown by the 6-311G(3d,2p) h_v and χ_v^{eq} values indicates that potential energy coupling between the OH local stretch and the torsional motion is sufficient to explain the paradoxical increase in the trans barrier in H_2O_2 upon OH overtone excitation and that the role of KE-coupling effects must be relatively minor in this case.

IV. Estimation of the Errors Present in the Computed h_v and χ_r^{eq}

A. Errors in $h(R)$ and χ_R^{eq} Due to Incomplete ab Initio Treatment. The strong sensitivity of the magnitude of the trans barrier $h(R)$ and equilibrium torsional angle χ_R^{eq} to increasing numbers of polarization functions (as seen in Figures 1 and 2) naturally leads one to wonder about the effect of further basis set expansion beyond the 6-311G(3d,2p) level. Likewise, the short O–O bond length computed at the MP2/6-311G(3d,2p) level (1.450 Å vs the experimental value of 1.464 Å) and the corresponding overestimate of the trans barrier suggest that a better treatment of electron correlation is needed. In this section, we describe the results of calculations using larger basis sets than 6-311G(3d,2p) and the fourth-order MP method MP4SDTQ.[28] Assuming that the MP2+GVB/6-311G(3d,2p) $h(R)$ and χ_R^{eq} curves (Figure 4) represent the "best" theoretical values, the results of the MP4 and larger basis set calculations can be used to estimate the uncertainty remaining in these "best" curves.

(28) Krishnan, R.; Pople, J. A. *Int. J. Quantum Chem.* **1978**, *14*, 91–100.

TABLE X: Effect of Increasing Basis Set Size on the Computed Trans Barrier in H_2O_2 for Two Values of the Local OH Stretch R^a

R, Å	basis set	$h(R)$, cm^{-1}	$\Delta h(R)$, cm^{-1}
R_{eq}	6-311G(3d,2p)	438	0
	6-311G(4d,3p)	439	1
	6-311++G(3d,2p)	457	19
	6-311G(3df,3p)	470	32
	6-311++G(3df,3p)	489[b]	51
1.2	6-311G(3d,2p)	609	0
	6-311G(4d,3p)	606	−3
	6-311++G(3d,2p)	638	29
	6-311G(3df,3p)	678	69
	6-311++G(3df,3p)	707[b]	98

[a] Values for the R-dependent trans barrier $h(R)$ were computed with the MP2 method for the MP2/6-31G* geometries (see Table V). [b] Value estimated by assuming that the effects of including ++ and f functions are additive.

The additional basis sets[20] that were investigated correspond to inclusion of an additional d function polarization set [6-311G(4d,3p)],[29] inclusion of f functions, [6-311G(3df,4p)], and inclusion of additional diffuse sp functions [6-311++G(3d,2p)]. Table X shows the results of computing $h(R)$ for $R = R_{eq}$ and 1.2 Å at the MP2 level with each of the larger basis sets. Assuming that the effects of including ++ and f basis functions are additive, $h(R)$ at the 6-311++G(3df,3p) level can be estimated, as given in Table X. In each case, the geometry of H_2O_2 was fixed at the MP2/6-31G* optimized values. The error introduced by not reoptimizing the geometry is expected to be small (<20 cm^{-1}) on the basis of the changes in $h(R)$ upon reoptimization seen previously at the MP2 level.

The larger basis set $h(R)$ values presented in Table X indicate that increasing the basis set size steadily increases the trans barrier at both the equilibrium value of R and the stretched value, although the increase is almost twice as large for the stretched length (98 cm^{-1} vs 51 cm^{-1}). It is noteworthy that the addition of the fourth d function changes the trans barrier insignificantly for both values of R. Diffuse "++" functions have only a moderate effect (20–30 cm^{-1}) on the trans barrier, but adding a set of f polarization functions has an appreciable effect, particularly on the trans barrier for the stretched value of R (70 cm^{-1}). In general, expansion of the basis set leads to an increase in the trans barrier and would probably cause a decrease in the O–O bond length.

In order to test the sensitivity of the trans barrier to increasing electron correlation, we performed MP4SDTQ (fourth-order Møller–Plesset perturbation theory using configurations generated by up to quadruple excitations) calculations[28] on H_2O_2 in order to find $h(R)$ for the two values of R considered above. Unfortunately, calculations using the 6-311G(3d,2p) basis were not considered practical, and so we used the smaller 6-31G* and 6-311G(2d,p) basis sets. Because a greater degree of electron correlation is obtained at the MP4SDTQ level than at the MP2 level, we also investigated the effect of reoptimizing the O–O bond length on the trans barrier as opposed to simply taking the MP2 optimized geometry. Table XI shows the MP4SDTQ $h(R)$ values obtained for both the MP2/6-31G* and the partially optimized MP4 geometries. The MP4 geometry optimization consisted of fixing all the geometrical parameters at the MP2 optimized values and then computing the total energy for several (usually five) values of the O–O bond length. The minimum energy O–O bond length was then found by interpolating (via a cubic spline) between the computed points.

The $h(R)$ values presented in Table XI indicate that, relative to MP2, MP4SDTQ lengthens the O–O bond and slightly lowers (<10 cm^{-1}) the equilibrium trans barrier in direct opposition to the trend of increasing trans barrier with increasing basis set size. However, the MP4 $h(R)$ value increases by about 20 cm^{-1} relative to the MP2 value when R = 1.2 Å. Using the 6-31G* and

(29) The polarization set (4d,3p) is not standard in GAUSSIAN 82. The values of the four d exponents were found by extending the even-tempered series used by Frisch et al. (ref 20) to build the 2d and 3d sets. The exponents of the three p hydrogen polarization functions were found in the same fashion.

TABLE XI: Effect of Increasing Electron Correlation on the Computed Trans Barrier in H_2O_2 for Two Values of the Local OH Stretch R^a

			MP2/6-31G* geometry		optimized geometry	
R	basis set	method	$h(R)$	$\Delta h(R)$	$h(R)$	$\Delta h(R)$
R_{eq}	6-31G*	MP2	210	0	210	0
		MP4SDTQ	204	−6	204[b]	−6
	6-311G(2d,p)	MP2	312	0	312	0
		MP4SDTQ	314	2	302[b,c]	−10
1.2	6-31G*	MP2	361	0	361	0
		MP4SDTQ	382	21	382[b]	21
	6-311G(2d,p)	MP2	469	0	477	8
		MP4SDTQ	481	12	485[b]	16

[a] Values for the R-dependent (R, Å) trans barrier $h(R)$ (in cm^{-1}) are given for two basis sets, with and without geometry optimization. [b] The O–O bond length, R_{OO}, was the only parameter optimized. All other geometrical parameters were fixed at the MP2 optimized values. [c] The optimized value of R_{OO} was found to be 1.468 Å, which is longer than the MP2 value by 0.013 Å. See the last paragraph in section III.A of the text.

6-311G(2d,p) MP4 $h(R)$ values, we estimate the MP4 correction to the "best" MP2/6-311G(3d,2p) trans barrier to be about −15 cm^{-1} for $R = R_{eq}$ and 20 cm^{-1} when $R = 1.2$ Å.

The combined effect of increasing basis set size and higher levels of electron correlation results in changes in $h(R)$ of about 40 cm^{-1} at R_{eq} and 120 cm^{-1} when $R = 1.2$ Å. From these values, we assign an uncertainty of ±50 cm^{-1} to the small R portion (0.5 Å $< R < R_{eq}$) of the "best" $h(R)$ curve, assuming extra uncertainty for further basis expansion, greater electron correlation, etc. Due to the greater variability in the computed $h(R)$ at $R = 1.2$ Å, we assume the uncertainty at the point to be ±150 cm^{-1}, and the uncertainty is taken to smoothly increase between R_{eq} and $R = 1.2$ Å.

Estimation of the uncertainty in the GVB part of the "best" $h(R)$ curve ($R > 1.2$ Å) is more difficult due to lack of calculations to guide the choice. Because the 6-31G* and 6-311G(2d,p) GVB $h(R)$ curves (see Figure 3) have the same basic shape as the corresponding MP2 curves, we assume that enhancements of the computational method (enlarging the basis, increasing electron correlation, etc.) will have the same effect on the GVB $h(R)$ values as on the MP2 $h(R)$. Taking into account that the MP2 $h(R)$ curve was found to become more uncertain as R increases, we chose a relatively large uncertainty, ±300 cm^{-1}, for $h(R)$ at $R = 1.8$ Å, twice the uncertainty at $R = 1.2$ Å, with the uncertainty increasing linearly between the two values of R.

Figure 6a shows the "best" [MP2+GVB/6-311G(3d,2p)] theoretical $h(R)$ curve and the estimated uncertainty as a function of R. The figure indicates that even though the uncertainty is fairly large (~±120 cm^{-1}), the basic feature of an increasing trans barrier with increasing OH stretch is relatively unaffected.

Estimation of the uncertainty remaining in the "best" χ_R^{eq} curve is much more arbitrary due to the lack of completely optimized geometries for basis sets larger than 6-311G(3d,2p) or computed with the MP4SDTQ method. We make use of the observation that the change in χ_R^{eq} is proportional to the change in $h(R)$ when the basis set is enhanced although the exact proportionality constant is dependent upon the value of the local OH stretch R. Examination of the MP2 optimized geometries and trans barriers given in Tables V and VII indicates that changes of about 30 cm^{-1} in $h(R)$ correlate well with 1° of change in χ_R^{eq} when $R = R_{eq}$, while the proportionality constant is 37 cm^{-1}/deg when $R = 1.2$ Å. The slight increase in the proportionality constant when $R = 1.2$ Å is a consequence of the fact that χ_R^{eq} becomes less uncertain as it asymptotically approaches 90° for large R. The correlation between changes in $h(R)$ and χ_R^{eq} suggests that uncertainties in "best" χ_R^{eq} curve can be assigned by simply considering them to be proportional to uncertainties in the "best" $h(R)$ curve. We therefore estimate the uncertainty for the small R part (0.5 Å $< R <$ 1.2 Å) of the "best" χ_R^{eq} curve to be ±2° corresponding to the uncertainty of ±50 cm^{-1} over the same region of

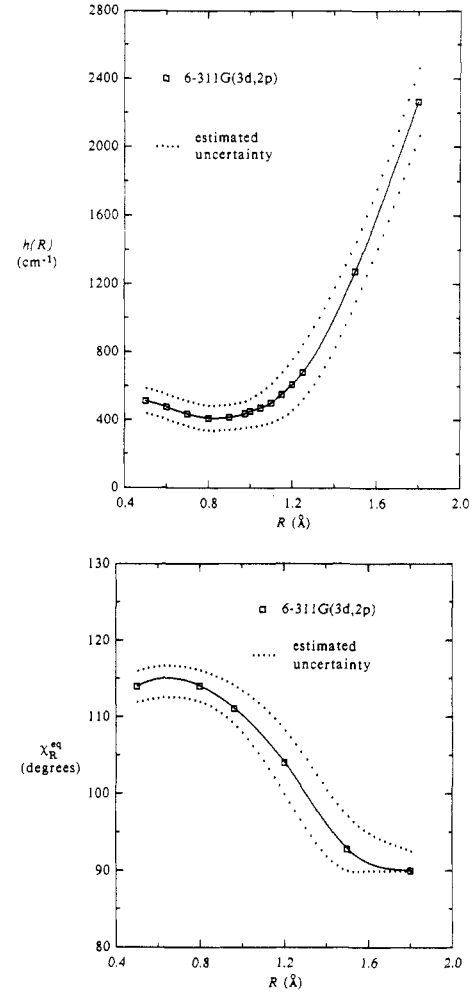

Figure 6. (a, top) "Best" theoretical trans barrier $h(R)$ in H_2O_2 as a function of the local OH stretch (given by the bond length R). The dotted lines indicate the estimated uncertainty in the computed $h(R)$. See section IV of the text for a discussion of how the uncertainty was estimated. (b, bottom) "Best" theoretical equilibrium torsional angle χ_R^{eq} in H_2O_2 as a function of the local OH stretch, R. The dotted lines indicate the estimated uncertainty remaining in the computed χ_R^{eq} curve. See section IV.A of the text for a discussion of how the uncertainty was estimated.

$h(R)$. At $R = 1.2$ Å, the uncertainty in $h(R)$ increases to ±150 cm^{-1}, which leads to an uncertainty of ±4° in χ_R^{eq} at that value of R. The relatively large uncertainty assigned to the $R = 1.2$ Å point is partially a consequence of the joining and smoothing procedure used to graft the GVB/6-31G* curve on to the MP2/6-311G(3d,2p) curve in order to construct the continuous χ_R^{eq} curve. Although the large R part of the χ_R^{eq} curve was formed by such an approximate procedure, the uncertainty in this part of the curve is constrained by the requirement that χ_R^{eq} must eventually approach the 90° asymptote. We assume that the uncertainty at $R = 1.5$ Å is the same as at $R = 1.2$ Å (±4°) and that the uncertainty at 1.8 Å is even less (±2°). Figure 6b shows the "best" χ_R^{eq} curve and the associated uncertainty. Although the uncertainties are estimated to be fairly large, like the $h(R)$ curve, the basic dependence of χ_R^{eq} on R is relatively unaffected.

B. Errors in the Computed h_v and χ_v^{eq} Values. Vibrationally averaging the upper and lower limits to the $h(R)$ and χ_R^{eq} curves formed by the estimated uncertainties directly gives the estimated upper and lower limits to the h_v and χ_v^{eq} curves due to inaccuracies in the ab initio method. Figure 7a,b show the "best" h_v and χ_v^{eq} curves with the estimated uncertainties obtained in this fashion as compared with the experimental values reported by Dübal and Crim.[4] The lower uncertainty of the MP2 part of $h(R)$ (±50 cm^{-1}) leads to smaller uncertainty in h_0 (±75 cm^{-1}), and the more uncertain GVB part of $h(R)$ (±300 cm^{-1}) leads to fairly large uncertainty in h_6 (±150 cm^{-1}). Estimates of greater error in the

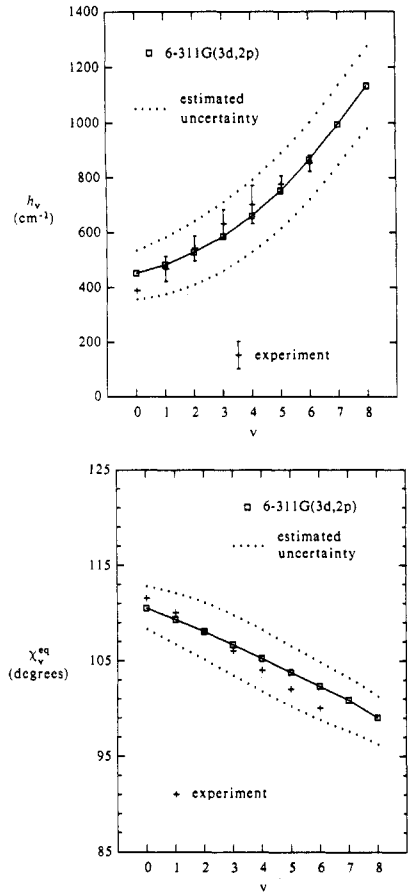

Figure 7. (a, top) "Best" theoretical (MP2+GVB/6-311G(3d,2p)) trans barrier h_v for the OH stretching overtone states (labeled by the quantum number v) in H_2O_2. The dotted lines indicate the estimated uncertainty remaining in the theoretical h_v. The experimental values shown were taken from text ref 4. (b, bottom) "Best" theoretical equilibrium torsional angle χ_v^{eq} for the OH stretching overtone states (labeled by the quantum number v) in H_2O_2. The dotted lines indicate the estimated uncertainty remaining in the computed χ_v^{eq} values. The experimental values shown were quoted from text ref 4.

GVB part of the curve have a large effect upon the uncertainty in h_v for high v, but have little effect upon the trans barrier in low overtone states (v = 0–4). The error in h_v for any v can be roughly estimated to be about ±100 cm^{-1}, although the error may be smaller for low v and larger for higher values of v. Likewise, the estimated uncertainty of the χ_v^{eq} curve is smallest for low levels of overtone excitation, but the bounds shown in Figure 7b also indicate that the uncertainty in χ_v^{eq} decreases for very high levels of excitation. This is due to the influence of the asymptotic part of the χ_R^{eq} curve on the higher overtone states. In both cases, good agreement is shown with experiment. Although the estimated uncertainties are fairly large, we believe that the uncertainty in the relative v dependence ("slope") of the curves is much smaller and that changes in the computational method are likely to lead to shifting of the "best" curve up or down within the bounds estimated here.

C. Errors Due to the Local Mode Model. Other uncertainties are implicit in the computed h_v and χ_v^{eq} values due to the local mode model assumed in the derivation of the equations defining h_v and χ_v^{eq}.

The error introduced by using Morse eigenfunctions rather than the eigenfunctions generated from the accurate OH stretching potential[30] to perform the vibrational averaging can be estimated by perturbation theory. Table I shows that the overtone frequencies derived from the Morse eigenvalues are within 60 cm^{-1} of the experimental values. From this, the difference between the Morse potential and the accurate potential is estimated to be small for R near equilibrium[30] but grows to be 100 cm^{-1} for R near 1.8 Å. Using this difference as the perturbation, we computed first-order corrections to the Morse eigenfunctions and used them to perform the averaging of $h(R)$, leading to changes in h_v of less than 10 cm^{-1}, indicating the insensitivity of the h_v values to small changes in the OH stretching wave function.

(30) The ab initio OH stretching potentials computed in this work agree well with the empirical Morse curve for small R (<1.4 Å), but severely underestimate the potential for large R (e.g. at R = 1.8 Å, the GVB/6-31G* value is about 25% too low). Ideally, the wave functions for the OH stretch used in the vibrational averaging would be derived from the computed potentials, but large errors would be introduced into the averaged values due to inaccuracies in the potential.

TABLE XII: Harmonic Vibrational Frequencies (in cm^{-1}) of the s' Modes of H_2O_2 Calculated at the MP2/6-31G* Level for the Equilibrium ($\chi = \chi^{eq}$) and Trans ($\chi = \pi$) Conformations

	MP2/6-31G* freq	
s' mode	$\chi = \chi^{eq}$	$\chi = \pi$
S_{rr} O–O stretch	929.0	928.4
$S_{\alpha\alpha}$ OOH bend	1461.1	1544.9
$A_{\alpha\alpha}$ OOH bend	1327.1	1257.7

Errors were also introduced in the computed values by neglecting various KE-coupling terms, for example, those embodied in $h_v^{(ho)}$ of eq II.22b. The contribution of the unexcited s′ modes can be estimated by computing the harmonic frequencies at the equilibrium and trans geometries. Table XII shows the frequencies for each of these conformations computed at the MP2/6-31G* level. Note that the table does not contain frequencies for the two OH stretching degrees of freedom, one of which belongs to the s′ set of coordinates. The frequencies of both modes are assumed to be independent of torsion, which is consistent with the local mode picture used in this work. In reality, frequencies were obtained for both symmetric and antisymmetric OH stretching modes, and the values of each were found to be nearly degenerate (within 8 cm^{-1}), indicating the aptness of the local mode picture. Using the computed frequencies, $h_v^{(ho)}$ was found (via eq II.22b) to be very small (about 7 cm^{-1}).

It is clear from the good agreement of the "best" h_v and χ_v^{eq} curves with experiment that the local mode model is generally valid and that within such a model pure PE coupling terms are sufficient to describe the observed dependence of the torsional potential on the state of overtone excitation.

V. Summary and Conclusions

We have investigated the coupling of torsion and OH overtone vibrations in hydrogen peroxide by high-level ab initio calculations, obtaining good agreement with the experimental observations of Dübal and Crim concerning the *increase* of the trans barrier with increasing levels of overtone excitation. Although such an increase appears paradoxical from a "Pauli repulsions" picture of barrier origins, we find that the effect is well reproduced in terms of potential energy coupling terms (of electronic origin) between separable torsion–vibration states in a local mode framework. Thus, our calculations provide support for the separability of torsional and vibrational motions and the general validity of the local mode description of OH overtone excitations which has generally been assumed in experimental analysis of H_2O_2 overtone spectra. Kinetic energy ("Born–Oppenheimer breakdown") coupling effects are not necessary to understand the general phenomenon of vibrationally enhanced barriers in H_2O_2.

We have shown how ab initio evaluation of the v-dependent trans barrier and torsional angle can be dramatically simplified in the local mode framework, reduced to quadratures over two one-dimensional slices through the full six-dimensional potential energy surface. This reduction makes it feasible to employ the highly polarized extended basis sets, a high level of correlation treatment, and full geometry optimization that are needed to describe the torsional properties of H_2O_2 in satisfactory quantitative terms, within present experimental uncertainties. "Triply polarized" basis sets are found to be necessary to give a quantitative description of the H_2O_2 equilibrium geometry, but the role of additional d or f functions is relatively minor. Our calculations with a variety of basis sets indicate that whereas the *magnitudes* of the $h(R)$ and χ_R^{eq} curves are very sensitive to the number of d

functions, the general *shape* of these quantities (leading to the observed v-dependence of the trans barrier and equilibrium torsional angle) is adequately represented at much lower basis set levels. Thus, overtone enhancement of the torsional barrier is indicated to be a fairly low-level qualitative feature of the H_2O_2 potential energy surface.

In the following paper, we employ the natural bond orbital (NBO) procedure to analyze the major electronic interaction that leads to the trans barrier and how that interaction is strengthened by stretching one of the OH bonds.

Registry No. H_2O_2, 7722-84-1.

Torsion–Vibration Interactions in Hydrogen Peroxide. 2. Natural Bond Orbital Analysis

J. E. Carpenter and F. Weinhold*

Theoretical Chemistry Institute and Department of Chemistry, University of Wisconsin—Madison, Madison, Wisconsin 53706 (Received: November 2, 1987)

In the preceding paper, we showed how the observed increase of the trans barrier in hydrogen peroxide upon OH overtone excitation can be calculated on the basis of potential energy coupling terms (of electronic origin) between the torsional and local OH stretching modes. In this paper, we investigate the nature of the potential coupling terms via the natural bond orbital procedure. The trans barrier and its vibrational enhancement are found to be primarily associated with charge-transfer interactions (hyperconjugation) between oxygen lone pairs and vicinal OH antibonds, as previous work on other ethane-type barriers would suggest. However, we also find an unusual contribution to the torsional potential (particularly, the cis barrier) which can be associated with electronic strain or "bond bending" in the axial O–O bond, and whose description is very sensitive to the inclusion of d functions. The d-orbital contribution to the O–O bond "kink" in turn has an indirect effect on the trans barrier. This appears to resolve the puzzling dependence of the peroxide barrier on d functions, which are necessary for the appearance of a trans barrier in the ground vibrational state but contribute negligibly to its vibrational enhancement.

I. Introduction

Recent experiments have shown that the trans barrier in hydrogen peroxide increases upon excitation of the OH overtone vibration.[1] In the preceding paper[2] (referred to as paper 1 here), we showed that this surprising observation can be numerically reproduced on the basis of potential energy coupling alone within a Born–Oppenheimer separation framework, thus providing support for the general separability of the torsion from the other higher frequency vibrations as well as for a local mode model of the OH overtone states. In this paper, we discuss the electronic nature of the potential energy coupling via the natural bond orbital (NBO) procedure.[3] This procedure provides an efficient method for finding a compact set of bonds and lone pairs for a molecule from the density obtained by ab initio calculations.

From our previous work and the work of others,[4] it is known that the shape of calculated torsional potential (and hence the trans barrier) is strongly dependent upon the composition of the basis set used, particularly the number of polarization functions. Figure 1 shows the torsional potential $V^{eq}(\chi)$ computed with the RHF method at three basis set levels: 6-311G, 6-311G(d), and 6-311G(2d,p).[5] Table I gives the optimized geometries and total energies found by the calculations used to generate the curves. The strong dependence of the torsional potential on the number of d functions is clearly evident in the figure. It is a striking feature of H_2O_2 that the extreme sensitivity of the torsional potential to the basis set is reproduced at all levels of theory—both correlated and uncorrelated. This suggests that polarization functions enter the electronic structure of the molecule in a very basic way. One of the questions we address in this work is exactly what role these functions play in determining the torsional potential.

Figure 2 shows the RHF/6-311G(2d,p) torsional potential as compared with the experimental torsional potential found by Hunt and co-workers.[6] It is clear that the calculated potential is in

TABLE I: RHF Optimized Geometrical Parameters and Total and Relative Energies [Giving the Torsional Potential $V^{eq}(\chi)$] of H_2O_2 as a Function of the Torsional Angle χ[a]

χ, deg	R_{OO}, Å	R_{OH}, Å	α_{OOH}, deg	total energy, au	$V^{eq}(\chi)$, kcal/mol
			RHF/6-311G Optimized Parameters		
0.0	1.4396	0.9531	108.99	−150.742 015 0	10.99
30.0	1.4365	0.9531	108.22	−150.744 818 3	9.24
60.0	1.4310	0.9528	106.52	−150.751 059 1	5.32
90.0	1.4297	0.9516	104.81	−150.756 490 1	1.91
120.0	1.4345	0.9503	103.33	−150.759 018 4	0.32
150.0	1.4394	0.9494	102.32	−150.759 534 5	0.00
156.0	1.4401	0.9493	102.19	−150.759 541 1	0.0[b]
180.0	1.4414	0.9492	101.96	−150.759 524 6	0.01
			RHF/6-311G(d) Optimized Parameters		
0.0	1.3910	0.9416	107.85	−150.790 850 0	9.86
30.0	1.3876	0.9419	107.15	−150.793 895 8	7.95
60.0	1.3818	0.9422	105.64	−150.800 377 3	3.88
90.0	1.3806	0.9416	104.17	−150.805 297 2	0.80
117.3	1.3845	0.9407	103.02	−150.806 567 0	0.0[b]
120.0	1.3851	0.9406	102.91	−150.806 558 5	0.01
150.0	1.3911	0.9400	101.92	−150.805 792 5	0.49
180.0	1.3936	0.9399	101.53	−150.805 260 0	0.82
			RHF/6-311G(2d,p) Optimized Parameters		
0.0	1.3965	0.9429	106.76	−150.811 680 0	8.17
30.0	1.3935	0.9434	106.14	−150.814 265 3	6.53
60.0	1.3881	0.9441	104.79	−150.819 738 4	3.10
90.0	1.3870	0.9438	103.43	−150.823 825 0	0.53
112.1	1.3894	0.9432	102.53	−150.824 671 4	0.0[b]
120.0	1.3904	0.9430	102.27	−150.824 587 3	0.05
150.0	1.3964	0.9425	101.39	−150.823 446 8	0.77
180.0	1.3985	0.9424	101.01	−150.822 744 7	1.21

[a] Values are given for three basis set levels. [b] Fully optimized structure.

(1) Dübal, H.-R.; Crim, F. F. *J. Chem. Phys.* **1985**, *83*, 3863–3872.
(2) Carpenter, J.; Weinhold, F. *J. Phys. Chem.*, preceding paper in this issue.
(3) Foster, J. P.; Weinhold, F. *J. Am. Chem. Soc.* **1980**, *102*, 7211–7218. Reed, A. E.; Weinhold, F. *J. Chem. Phys.* **1983**, *78*, 4066–4073. Reed, A. E.; Weinstock, R. B.; Weinhold, F. *J. Chem. Phys.* **1985**, *83*, 735–746.
(4) Dunning, T. H.; Winter, N. W. *J. Chem. Phys.* **1975**, *63*, 1847–1855. See also Cremer, D. *J. Chem. Phys.* **1978**, *69*, 4440–4455.
(5) All calculations were carried out with the VAX (revision H) version of GAUSSIAN 82. This programs was developed by J. S. Binkley, M. J. Frisch, D. J. Defrees, K. Ravhavachri, R. A. Whiteside, H. B. Schlegal, E. M. Fluder, and J. A. Pople (Carnegie-Mellon University, Pittsburgh, PA). 6-311G: Krishnan, R.; Binkley, J. S.; Seeger, R.; Pople, J. A. *J. Chem. Phys.* **1980**, *72*, 650–654. (df,p) supplementary functions: Frisch, M. J.; Pople, J. A.; Binkley, J. S. *J. Chem. Phys.* **1984**, *80*, 3265–3269.

0022-3654/88/2092-4306$01.50/0